Electronic Supplementary Information (ESI)

Stimuli-Responsive Anisotropic Actuation of Melem-Formaldehyde Polymer

Yang Wang, †[a] Niannian Wu, †[a] Congyan Liu,[a] Mohamed K. Albolkany,[a] Min Wang,[a] Yan Wang,[a] Syeda Arooj,[a] Wenhua Zhang,[b] and Bo Liu[a]*

[a]Hefei National Laboratory for Physical Sciences at the Microscale, Fujian Institute of Innovation of Chinese Academy of Sciences, School of Chemistry and Materials Science, University of Science and Technology of China, Hefei, Anhui 230026, China.

[b]National Synchrotron Radiation Laboratory, Anhui Provincial Engineering Laboratory of Advanced Functional Polymer Film, University of Science and Technology of China, Hefei, Anhui 230029, China

*Correspondence to: liuchem@ustc.edu.cn.

Table of Contents

1. Experimental Section

1.1 Chemicals and materials

Melamine ($C_3H_6N_6$, 99%) and paraformaldehyde (PF, AR) were purchased from Shanghai Macklin Biochemical Co. Ltd. (China). Sulfuric acid-d_2 (96-98 wt% in D_2O) was purchased from Energy Chemical; dimethyl sulfoxide-d_6 was purchased from Adamas-Beta. Sodium hydroxide (NaOH, AR, ≥96%), concentrated sulfuric acid (H_2SO_4, 95-98%), dimethyl sulfoxide (DMSO, AR, ≥99%), acetone (AR, ≥99.8%) and methanol (AR, ≥99.5%) were purchased from Sinopharm Chemical Reagent Co., Ltd. (Shanghai, China) and used without further purification.

1.2 Preparation of melem

Melem was prepared according to a modified literature process.[1] Specifically, 5 g melamine was loaded into a loosely covered crucible and then heated to 450 ^oC for 5 h at a ramping rate of 1 ^oC/min in a muffle furnace in air. After cooling down to room temperature with a rate of 3 ^oC/min, white beige melem was obtained.

1.3 Preparation of melem-H

Melem (500 mg) was dispersed into 10 mL H_2SO_4, followed by heating at 80 ^oC for 12 h under stirring to form pale yellow solution. White powder was precipitated from the above solution by adding polar solvent of methanol, which was further washed with methanol and dried at 60 ^oC for 12 h. The resultant powder (denoted as melem-H) was capable of dissolving in DMSO with solubility > 50 mg/mL at room temperature.

1.4 Preparation of MF solution and MFF

The as-prepared melem-H powder (500 mg) was dissolved in 20 mL DMSO at room temperature, followed by adding with 413 mg PF and 300 μL NaOH (10 wt%). The resultant suspension was then heated at 80 ^{o}C for 12 h under stirring to form colorless solution, and there is no precipitate after cooling down to room temperature. Subsequently, 10 mL solution was then subjected to further heating at 100 ^{o}C for 3 h in oven to obtain transparent film, which can be readily peeled off for further tests. The briefly descried procedures for MFF formation are completed under optimized conditions, the process optimization in more details will be discussed in Section 2.2.

1.5 Characterization

X-ray diffraction (XRD) measurements were performed on a Rigaku MiniFlex 600 X-ray diffractometer with Cu Kα radiation (λ = 1.54178 Å). X-ray photoelectron spectra (XPS) were recorded on an ESCALab 250 high-performance electron spectrometer using monochromatized Al Kα radiation (*hv* = 1486.7 eV) as the excitation source. Fourier transform infrared (FT-IR) spectra were performed on a SHIMADZU IR Affinity-1 spectrometer with KBr discs in a range from 4000 to 400 cm^{-1}. Microstructural observation of studied samples was completed with field emission scanning electron microscope (FE-SEM, Zeiss Supra 40, equipped with energy dispersive spectrum (EDS)) at an acceleration voltage of 5 kV and atomic force microscope (AFM) by means of Veeco DI Nanoscope MultiMode V system. The CP-MAS ^{13}C-NMR measurements were carried out with a Bruker AVANCE AV III 400WB spectrometer operating at 400 MHz. Elemental analyses of C, N, O and S

were conducted on a Vario EL Cube elemental analyzer. Thermogravimetric analyses were performed from 25 to 800 ^{o}C at a heating rate of 10 ^{o}C/min in air atmosphere on a TGA Q500 integration thermal analyzer. Mechanical properties of MFF were tested on an Instron 3340 universal testing instrument at 25 °C, with a relative humidity of 51 ± 2%. The anisotropy of MFF was probed using near edge x-ray absorption fine structure (NEXAFS) spectroscopy at the BL12b beamline of National Synchrotron Radiation Laboratory (Hefei, China). The linear polarity of this bending magnet beamline is about 90% and the beam size on sample is approximately 1.5 × 1 mm^2. During the measurement, the incidence X-ray remained normal to the membrane surface so that the electric field vector of the beam was parallel to the sample surface. C K-edge and N K-edge were recorded with the sample locating at two orthogonal azimuthal angles so that the electric field vector is parallel with or perpendicular to the textile direction of MFF.

2. Discussion on the formation process of MFF

2.1 Discussion on the preparation of melem-H and characterizations

Melem (2,5,8-triamino-tri-*s*-triazine) was frequently referred to as an intermediate phase during the formation of graphitic carbon nitride (g-CN) via polymerization of cynamide.[1,2] It was found that melem was insoluble in most common solvents (H_2O, C_2H_5OH, CH_3OH, DMF, CH_3CN, acetone, etc.) and only dissolved in DMSO with a very limited solubility, which was evidently lower than melamine (2,4,6-triamino-*s*-triazine) but higher than chemically inert g-CN. This fact strongly suggests that more extended conjugated structure gives rise to lower solubility. Previous reports demonstrated that g-CN could be dissolved and form true thermodynamic solution in concentrated sulfuric acid, which has been employed in addressing the insolubility of graphitic materials.[3-5] In this work, the solubility of melem in H_2SO_4 was investigated. As expected, pale-yellow solution can be formed at 80 ^oC and kept unaltered after being cooled down to room temperature (labeled as melem-H solution). The determined solubility can be higher than 385 mg/mL at room temperature. Along with this, the structural stability of melem in H_2SO_4 was a major concern and confirmed using liquid-state ^{13}C-NMR spectra, as shown in Fig. S1. The solid-state ^{13}C-NMR spectra of melam, melamine-melem adduct, melem, and melon in previous reports showed that the chemical shift of corner carbons in carbon nitrides were about 10 ppm higher than that of bay carbons.[2,6,7] Thus, the observed resonances 1 (155.6 ppm) and 2 (147.0 ppm) can be reasonably assigned to the corner carbons and bay carbons, respectively (Fig. S1).

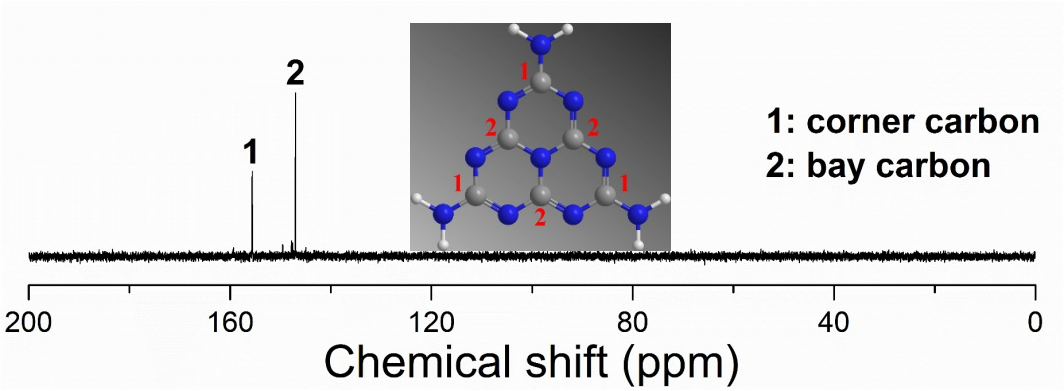

Fig. S1 Liquid-state ^{13}C-NMR spectra of melem-H solution (dissolved in d_2-H_2SO_4).

We further attempted to precipitate the melem-H solution via adding aprotic polar solvents (H_2O, CH_3OH, etc.). The white powder was then thoroughly washed with methanol and dried at 60 ^oC for 12 h to get dry melem-H powder. The structural stability of melem in melem-H was confirmed using liquid-state ^{13}C-NMR spectra, as shown in Fig. 2A in main text. Also, the two resonances 1 (161.4 ppm) and 2 (152.3 ppm) can be well assigned to the corner carbons and bay carbons of melem unit, respectively. Note that the chemical shifts of melem in d_2-H_2SO_4 are slightly different from those of melem-H in d_6-DMSO owing to the solvent effect. Prior to further reaction using melem-H powder, the solubility of melem-H in DMSO was found to be higher than 50 mg/mL at room temperature, far exceeding that of pristine melem. All these findings potentially endowed melem-H with solution-processed reactivity.

2.2 Discussion on the formation of melamine-formaldehyde polymer

Melamine can be cross-linked by reacting with formaldehyde (HCHO) in acidic or basic conditions, forming polymer networks (Fig. S2A) for various task-specified applications.[8-10] Typically, melamine prefers to react with HCHO and form multi-methylol group with assistance of base (pH = 8-9). Depending on the varying molar

ratio between melamine and formaldehyde, different products would be obtained, such as trimethylol- and hexamethylol-based melamine (Figs. S2B and S2C). Subsequently, the condensation of methylols can be initiated under acidic condition (pH=5-6) in various ways (Figs. S2D and S2E), upon which methylol can form ether bond via dehydration, resulting in the formation of -$NHCH_2OCH_2NH$-bridged framework. Further dehydration would give rise to the formation of -$NHCH_2NH$-bridged framework. The pH value of reaction system, molar ratio of melamine to formaldehyde and solid content are important factors that dominate the reaction. All the procedures are completed using water as solvent.

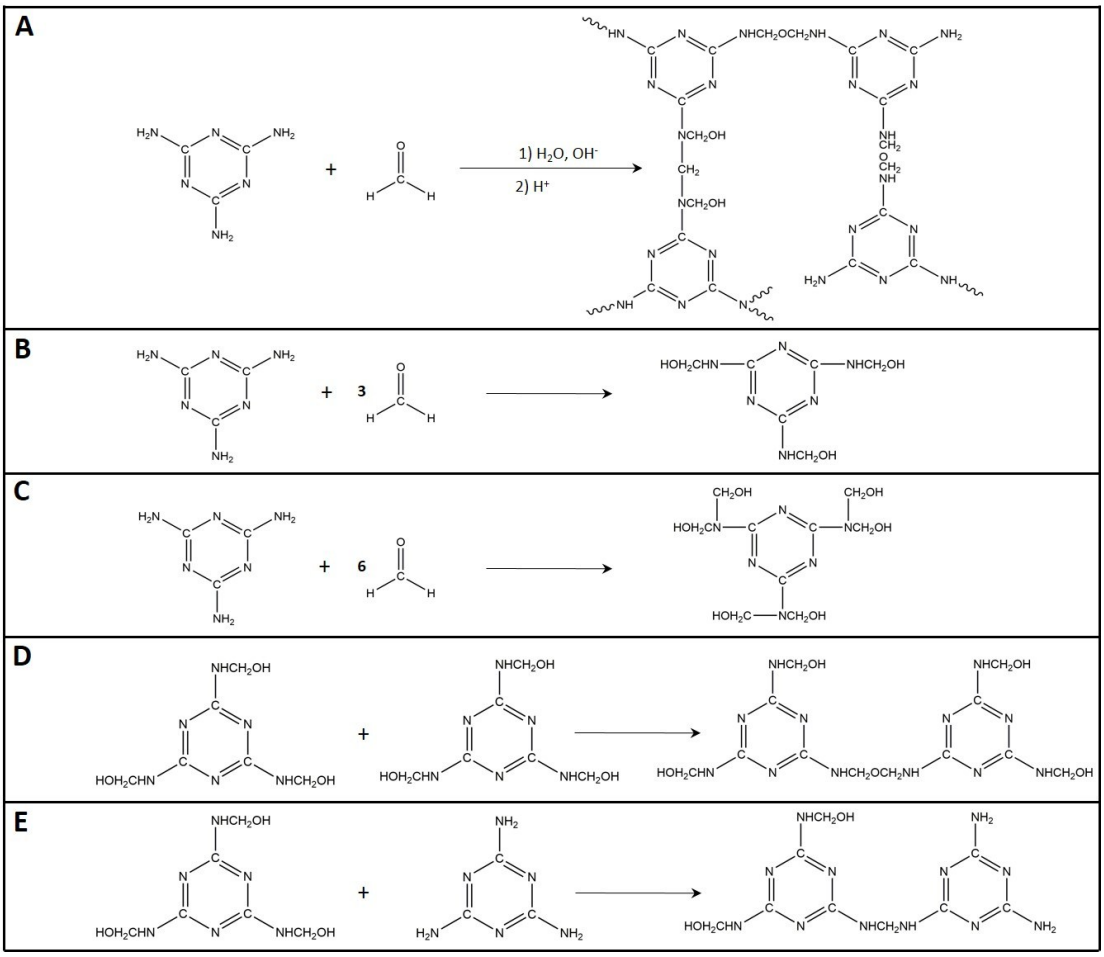

Fig. S2 Various reactions between melamine and formaldehyde (HCHO).

(A) Formation of melamine-HCHO polymer under basic and acidic conditions.

(B) Formation of trimethylol-based melamine under basic condition (melamine: HCHO=1:3, in molar ratio).

(C) Formation of hexamethylol-based melamine under basic condition (melamine: HCHO=1:6, in molar ratio).

(D and E) Formation of -$NHCH_2OCH_2NH$- or -$NHCH_2NH$- bridged framework under acidic condition.

2.3 Discussion on the MFF formation process

As mentioned above in Section 1.4, the reaction between melem-H and PF contributed to the formation of colorless solution (MF solution) at a relatively low temperature of 80 ^{o}C. Elevating the temperature to 100 ^{o}C under vacuum resulted in the formation of colorless film suspended in light-blue suspension within 24 hrs. It was found that increasing the concentration of initial reactants by one-fold would facilitate film formation within 6 h with unaltered reaction conditions. With further effort to realize fast formation of film, we transferred 10 mL as-obtained colorless solution (formed at 80 ^{o}C) into a watch glass (diameter: 60 mm) with smooth surface, followed by uniform heating in oven at 100 ^{o}C. Well-developed colorless film with regular texture can be formed within 2 h and readily peeled off, upon which the thickness can be adjusted by changing the volume of the solution.

As clearly shown in Fig. S3A, FT-IR spectra of all samples give evident peaks at ~805 cm^{-1} (tri-s-triazine ring out of plane bending) and 1300-1700cm^{-1}(C-N and C=N stretching vibrations), thus indicating the retained structure of melem after H_2SO_4 treatment.[11-13] The intensity and peak of the samples are slightly shifted with respect to those of melem. The shift are ascribed to the protonation of melem with H_2SO_4 and resultant less ordered structure.[14,15] Typically, S=O (1332, 1115 cm^{-1}) and S-O (1063, 973 cm^{-1})[14,16] vibrations assigned to SO_4^{2-} or HSO_4^{-} are identified in melem-H, while the peaks evolve into S-O vibrations that belong to $S_2O_7^{2-}$ (1263, 1046 and 585 cm^{-1}) in MFF.[16,17] This finding indicates the cross linking of SO_4^{2-} group into $S_2O_7^{2-}$ group (S-O-S vibration) during the formation of MFF, which is further verified by Raman

spectroscopic study of MFF (Fig. S4). Specifically, the emerged bands can be generally ascribed to the $S_2O_7^{2-}$-based compounds rather than SO_4^{2-}/HSO_4^--based species.[16] These data illustrate that the formation of S-O-S via SO_4^{2-}/HSO_4^- crosslinking takes place during the formation process of MFF. Also, C-H bending vibration (1380 cm^{-1})[18] is observed in FTIR spectra of both MF and MFF. However, the C-O vibration of ether (1017 cm^{-1})[19] is detected in MFF, thus distinguishing it from MF solution formed at 80 °C. The combined findings are in line with ^{13}C-NMR results as shown in Figure 2A in main text.

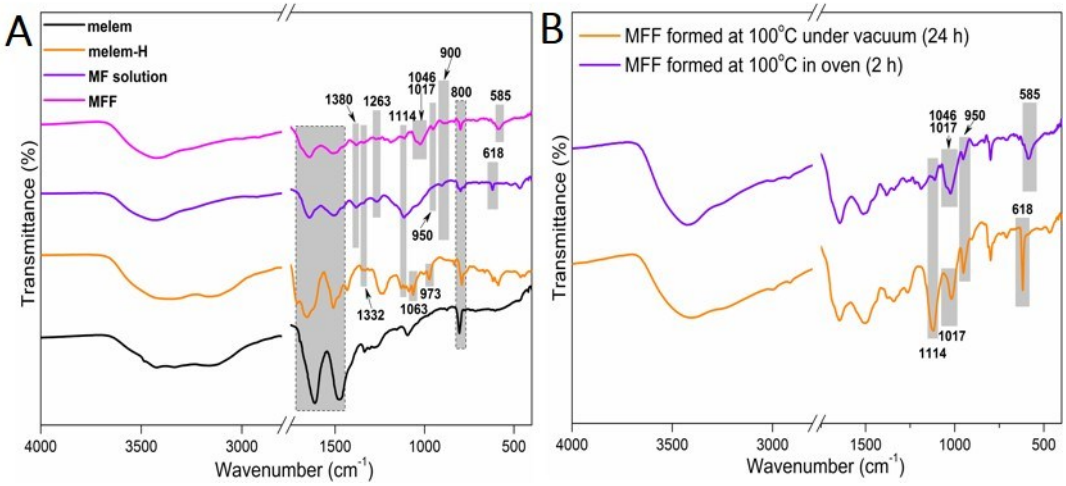

Fig. S3 (A) FT-IR spectra of melem, melem-H, MF solution and MFF. (B) FT-IR spectra of MFF formed at 100 °C under different conditions.

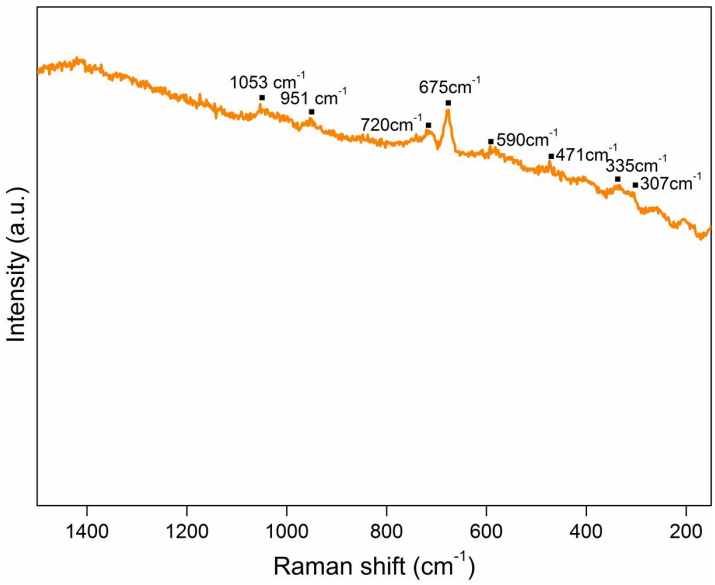

Fig. S4 Raman spectra of MFF formed at 100 °C in oven.

In addition, the FT-IR spectra shown in Fig. S3B demonstrates that MFF formed at 100 °C at different conditions share identical vibrations at 1017 cm^{-1}, indicating the formation of C-O ether in both cases.[19] However, the peaks located at 1114 cm^{-1} and 950 cm^{-1} that belong to S=O and S-O vibrations[5,16] in SO_4^-/HSO_4^- based compounds are less profound in MFF formed in oven (2 h) when compared with that formed under vacuum (24 h), while the emerged peak at 1046 cm^{-1} (S-O-S vibration)[16,17] in MFF formed in oven is more evident and overlapped with peak at 1017 cm^{-1}. Although the vibrations at both 618 cm^{-1} and 585 cm^{-1} can be assigned to S-O related vibrations[16,17] in sulfate-based compounds, the disappearance of 618 cm^{-1} and emergence of 585 cm^{-1} in MFF formed in oven (2 h) may indicate that the two peaks can be assigned to S-O and S-O-S vibrations, respectively. All these findings well explain the less regular texture of MFF formed under vacuum (24 h), due to the less cross-linking degree of S-O-S.

High-resolution XPS N1s, O1s and S2p spectra are also analyzed in details to

verify their chemical environment of MFF. Specifically, the four peaks of N 1s spectra in Fig. S5A confirm the existence of sp^2 hybridized nitrogen C-N=C at 398.8 eV (N1), the ternary nitrogen N-$(C)_3$ at 400.1 eV (N2), the amino functional groups C-N-H at 401.4 eV (N3). The N4 signal at 404.6 eV is generally ascribed to the positive charge localization in C-N heterocycles.[20] All N1s peaks are indicative of the retained tri-s-triazine framework in MFF. The S 2p spectra of MFF in Fig. S5B reveals the existence of sulfuric species and the signal can be de-convoluted into $2p_{1/2}$ and $2p_{3/2}$ (peak area=1:2), which confirms the existence of SO_4^{2-}.[21] Another peak at 166.3 eV is ascribed to the sulfoxide.[22] Note that no other sulfide species associated with lower valence states of sulfur are detected,[23] thereby suggesting a redox-free process during MFF formation. The O1s peaks of the MFF can be de-convoluted into two peaks for the SO_4^{2-} (O1, 531.70 eV)[21] and C-O ether (O2, 532.90 eV),[24] as clearly shown in Figure S5C. All signal assignments keep good consistency with that of NMR, FT-IR and Raman results.

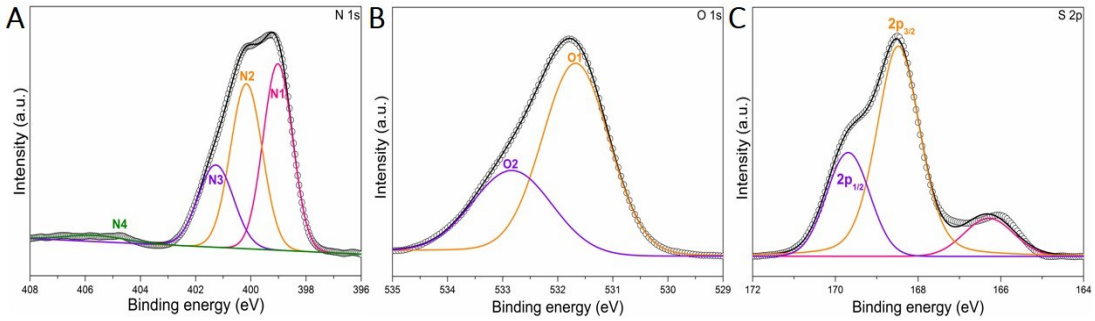

Fig. S5 High-resolution XPS N1s (A), O1s (B) and S2p (C) spectra of MFF.

We directed our research focus on the film formation process in more details. The initial melem-H powder and PF were controlled at lower concentrations in DMSO and subjected to the identical heating procedures to form colorless solution. Further heating at 100 ^{o}C in oven or under vacuum would first contribute to the formation of colorless threadlike one-dimensional MF polymer prior to two-dimensional MFF formation.

In addition, the SEM and EDS images of MFF shown in Fig. S6 clearly reveal that the S and O contents varied oppositely from top to bottom surface. As described in main text, two gradients (polymerization gradient and cross-linking gradient) exist along thickness direction. Such materials gradients formation might be caused by the concentration change of precursors during MFF film growth in a solution-based assembly process, associating with the different growth mechanisms of 1D chain polymerization and cross-linking of pyrosulfate component.

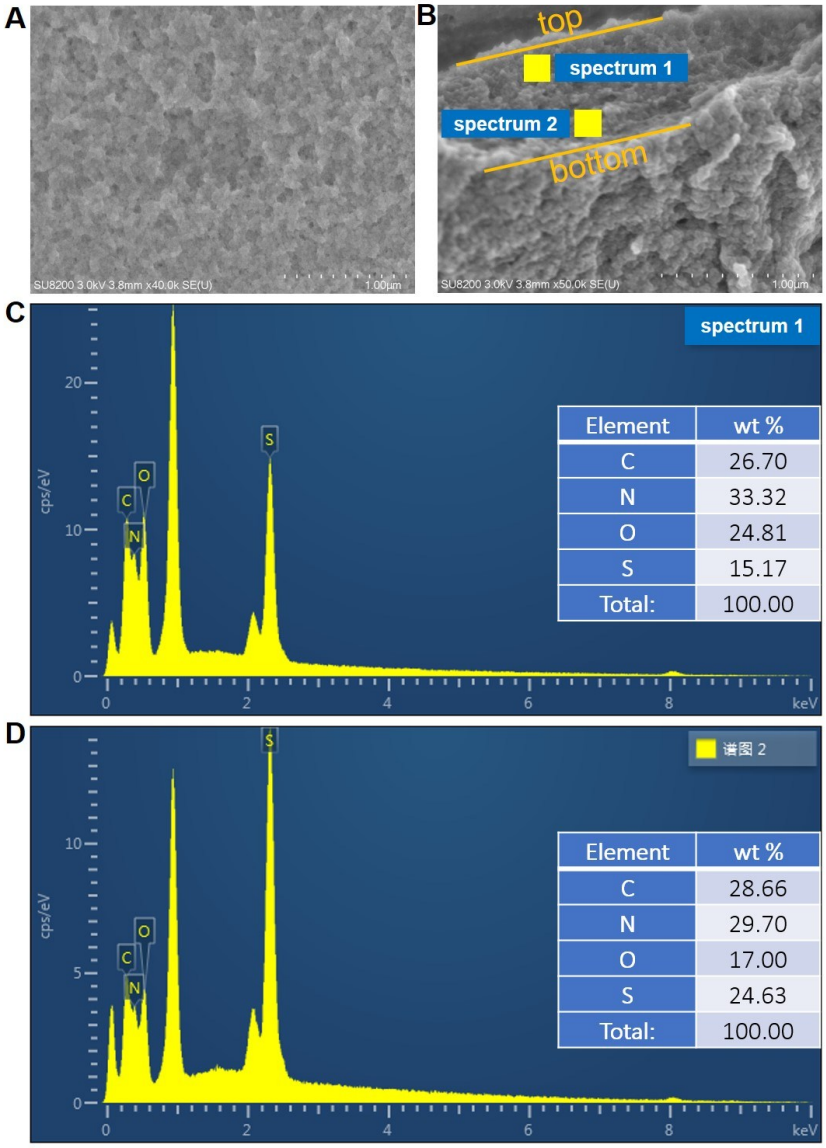

Fig. S6 Surface (A) and cross-sectional (B) SEM images of MFF. Energy dispersive spectrum (EDS) of points 1 (C) and 2 (D) highlighted in (B). Insets of (C) and (D) show the element compositions of points 1 and 2, respectively.

3. Video S1 description: MFF formation process

To present a better visual experience that enables us to clearly see the textile evolution recorded by smartphone, the content of starting materials utilized for the preparation of MFF were altered. Specifically, the mass of both melem-H and paraformaldehyde were increased by 4-fold by fixing the volume of DMSO and NaOH. The obtained MF solution at 80 ^{o}C functioned as precursor for MFF formation was therefore featured with much higher solid content, upon which the video of MFF formation process was recorded. As marked in Video S1, the played speed was 64-fold accelerated (real time: 35 min) and evident textile evolution can be observed. Higher solid content contributed to faster MFF formation, as previously illustrated in Section 2.3. The thickness and size of MFF can be reasonably controlled by changing the volume of MF solution and container sizes, respectively. Note that it is of difficulty to clearly record the formation of 1D threadlike polymer formation, which was picked out carefully and used for solvent vapor responsive experiments.

4. Probing anisotropy of MFF by different characterizations

4.1 Polarizing microscope

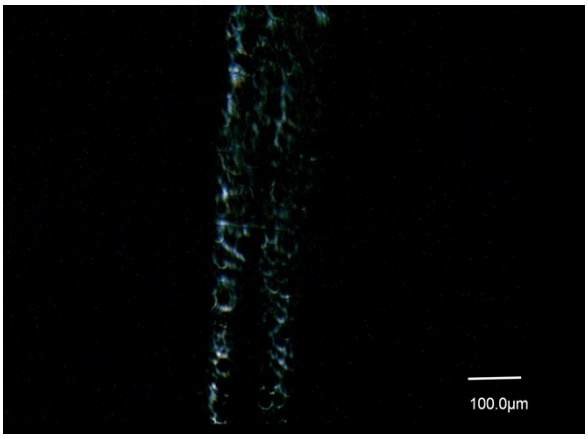

Fig. S7 Polarized light microscopic image of MFF.

4.2 Optical microscope

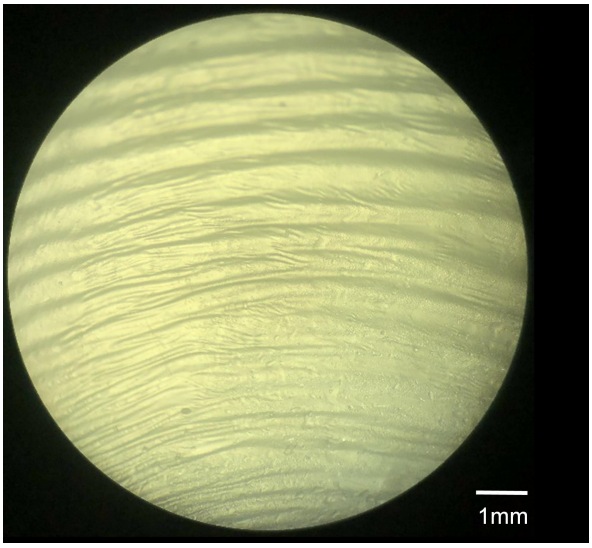

Fig. S8 Optical microscopic image of MFF.

5. Water and n-pentane vapor adsorption of MFF by quartz crystal microbalance (QCM)

5.1 Fabrication of MFF deposited on QCM crystals and Experimental set-up

The gold-coated quartz crystal was first cleaned by immersing into piranha solution (98% H_2SO_4 :30% H_2O_2, 3:1 v/v) for 5 min and rinsing with ultrapure water. The gold surface of the quartz crystal was dried under a stream of argon. MF solution (50 μL) was deposited onto the gold surface of a QCM crystal and then subjected to heating at 100 ^oC for 10 min to obtain a thin MFF layer. Prior to QCM detection, the automated QCM 200 (Princeton) was guided to smooth baseline under flowing nitrogen (99.9999% purity, 1 mL/min) at 45 ^oC. The adsorption tests were carried out after cooling down the temperature to 298 K under a flow rate of 1mL/min controlled by a flow meter. The experimental set-up is shown in Fig. S9.

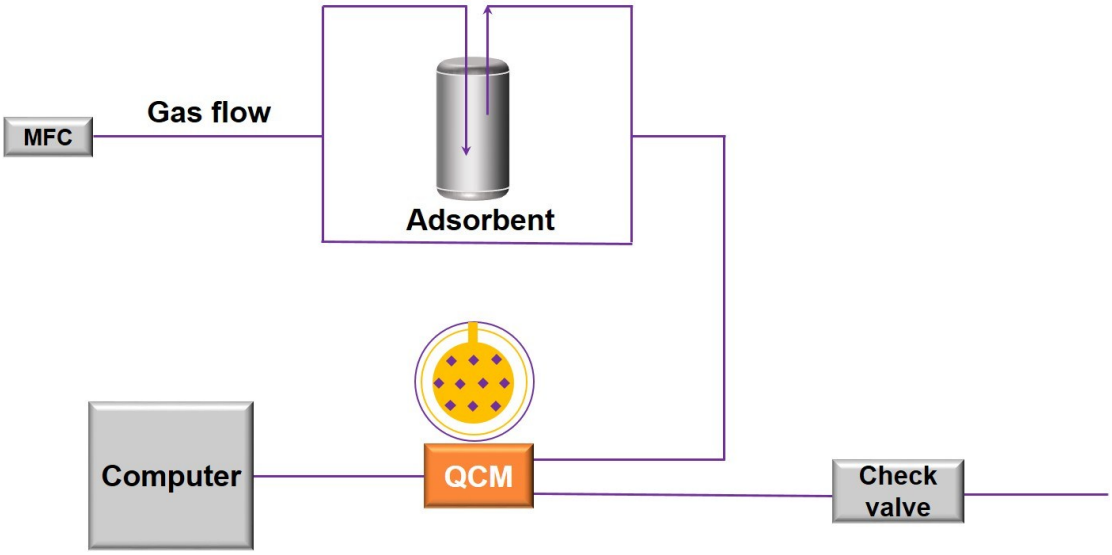

Fig. S9 Schematic illustration of the QCM measurement system for probing the adsorption of water or n-pentane vapor on MFF. (MFC: mass flow controller)

5.2 Quantitative analysis of experimental adsorption data obtained by QCM

QCM is capable of recording resonance frequency (f) and frequency change (Δf). They are interpreted by the Sauerbrey equation, which states that Δf is linearly proportional to the mass load at the crystal exposed surface:

$$\Delta f = \frac{2nf_0^2 \Delta m}{\sqrt{\mu_q \rho_q} A} = -C_f \frac{\Delta m}{A}$$

where f_0 is the fundamental resonant frequency, Δ_f is the frequency change due to mass loading, n is the harmonic number, ρ_q (2.648 g/cm^3) and μ_q (2.947 × 10^{11}g/cm/s^2) are the density and the shear mode of the quartz material, respectively, Δm is the mass change at the crystal surface, and A is the crystal sensitive area. C_f is a constant which only depends on physical parameters of the crystal.

The frequency change-time dependency was monitored with continuously flowing of the analyte vapor. The Mass uptake (M_t / M_e) is given by the following equation:

$$M_t/M_e = (f_t - f)/(f_e - f)$$

where M_t is the mass uptake at time t, M_e is the mass uptake at equilibrium, f_t is frequency of the oscillator at a time t, f is frequency of the oscillator at a $t = 0$ ($P/P_0 = 0$) and f_e is frequency of the oscillator at equilibrium.[25]

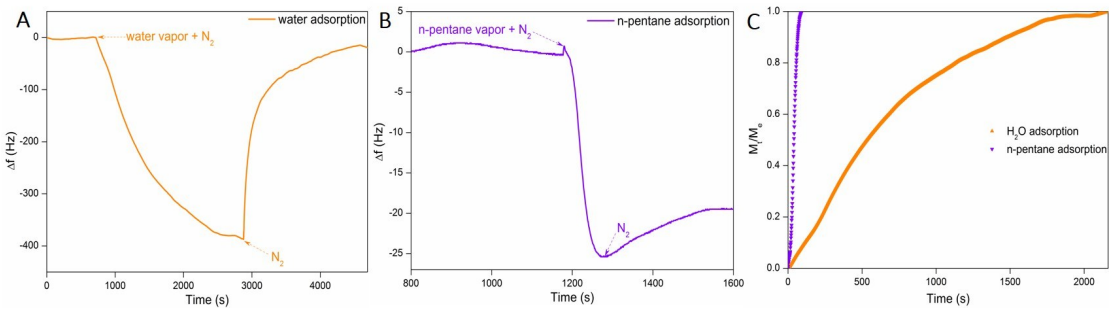

Fig. S10 Sorption of water and n-pentane vapor on MFF.

(A and B) Adsorption-desorption curves of MFF over water (A) and n-pentane (B) vapor recorded at 298 K.

(C) Time-dependent mass uptakes of MFF at 298 K for water and n-pentane.

6. Alternative ways to determine the adsorption of MFF

6.1 Contact angle test of MFF

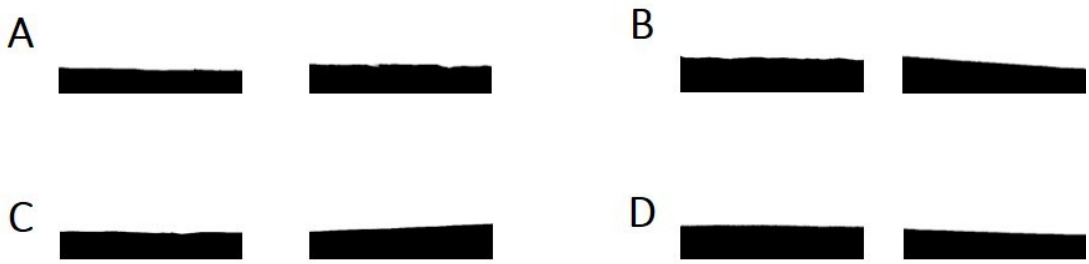

Fig. S11 Digital photos of (A) H_2O, (B) MeOH, (C) n-pentane and (D) DMSO droplets on front surface (left) and back surface (right) of MFF.

The front and back surfaces of all the obtained MFF exhibited zero contact angle over different solvents, demonstrating the solvophilic attribute of MFF over the solvents with varied polarity.

6.2 Experimental set-up for permeability evaluation of MFF

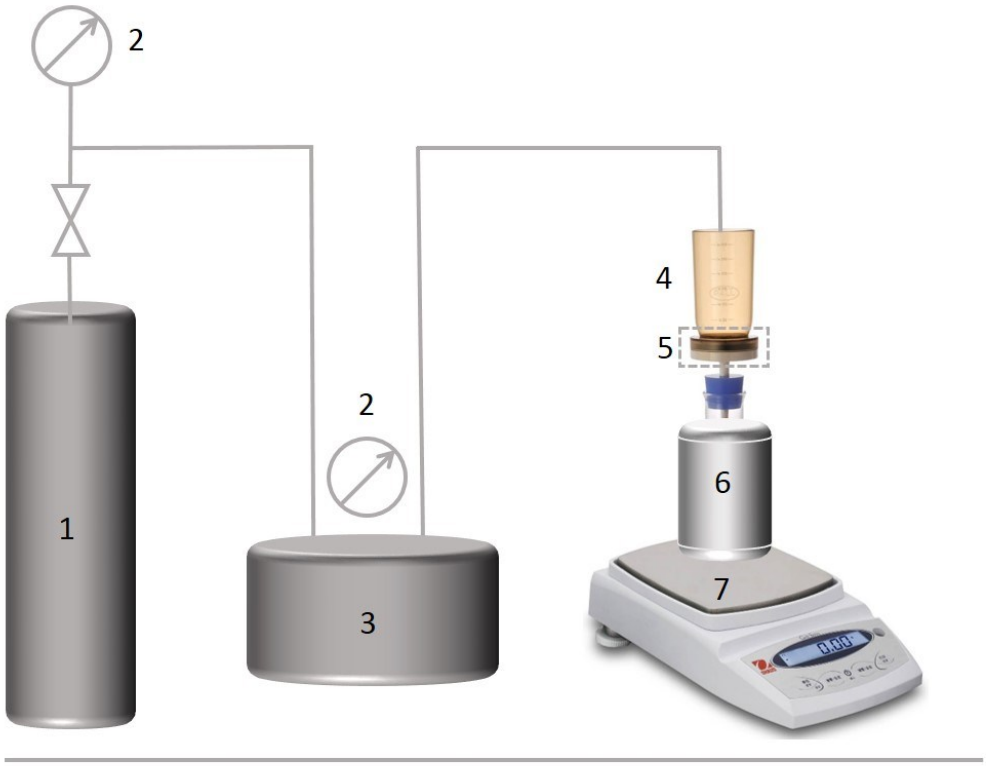

Fig. S12 Schematic diagram of dead-end filtration device.

We further evaluated the permeability of different liquids through MFF using the dead-end filtration device. As briefly schemed in Fig. S12, the applied pressure can be controlled with buffer tank, the permeated amount of liquid can be quantitatively analyzed using electronic balance. It was found that neither water nor n-pentane can permeate through MFF under externally applied pressure at 1-2 bar.

7. Video S2 and S3 description and mechanical properties of MFF

7.1 Video S2: Reversible anisotropic actuation of MFF in DMSO and MeOH

The as-obtained MFF was cut into a ~2x2 cm^2 fragment for video recording. As shown in Video S2, the film curled perpendicularly to texture direction upon immersion in DMSO and kept static upon reaching equilibrium. Next, we transferred the film into MeOH, where the film quickly curled back to its original shape and further curled along texture direction owing to DMSO-MeOH solvent exchange. Subsequently, the film was put back into DMSO, which underwent recovering and curling perpendicular to texture direction again during MeOH-DMSO solvent exchange. The video shows that the anisotropic actuation of MFF is reversible, robust responsiveness without obvious decay can be obtained after many cycles. Here we only show three cycles for demo with a 4-fold play speed.

7.2 Stress-strain profiles of MFF

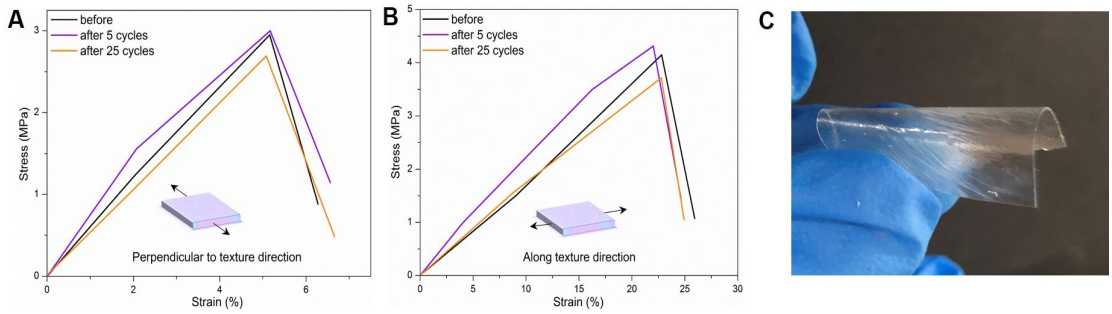

Fig. S13 Stress-strain profiles of MFF (before and after being exposed to solvents for 5 and 25 cycles) under a strain rate of 0.17/s, which are stretched (A) perpendicularly to and (B) along texture direction. (C) Digital photo of MFF after being exposed to different solvents and 25 cycles of anisotropic responses.

The freshly prepared MFF was cut into two 3×3 cm^2 fragments, both of which were further divided into three 3×0.5 cm^2 fragments along texture direction and perpendicular to texture direction, respectively. By this way, we guarantee that all samples from the same batch of MFF show no difference in sizes when recording the stress-strain profiles. The gauge length of all samples was around 10 mm prior to uniaxial tension. The mechanical properties of 2D MFF before and after being exposed to different solvents were studied via recording stress-strain curves, which are shown in Fig. S13. It is found that pristine MFF exhibits strain values of ~5.16 % and ~22.8 % for the film stretched perpendicularly to and along texture direction, respectively (Table S1). Also, the strain values of MFF after multi-cycles of anisotropic responses are comparable with that of pristine values, the strain values of MFF are generally around 5 % (stretching perpendicularly to texture) and 22 % (stretching along texture) after different cycles of anisotropic responses. The Young's

modulus (*E*) of MFF are determined to be 57.2 MPa and 18.2 MPa when stretching is perpendicular to and along texture direction, respectively (Table S1). After being exposed to different solvents and 5 cycles of anisotropic responses, the *E* values are 58.0 MPa and 19.6 MPa, respectively (Table S1). This is one or two orders of magnitude lower than that of bulk PVC (2700-3000 MPa)[26] and PCL (252-430 MPa)[27], the lower *E* values indicates that MFF is more prone to deform within appropriate stress range. Compared with the original values, MFF shows similar *E* values after 25 cycles of anisotropic responses (perpendicular to texture: 53.0 MPa, along texture: 16.3 MPa, Table S1). The negligible changes of both *E* and strain values of MFF before and after being exposed to solvents, indicating that the anisotropic responses upon interaction with solvents would not significantly alter the mechanical properties after external stimuli (Fig. S13C). Also, the different *E* values for MFF undergoes stretching along and perpendicular to texture direction again support its anisotropic nature.

Table S1 Mechanical parameters of MFF after different cycles of anisotropic responses.

Mechanical parameter	Pristine MFF	After 5 cycles	After 25 cycles
E (perpendicular to texture)	57.2 MPa	58.0 MPa	53.0 MPa
E (along texture)	18.2 MPa	19.6 MPa	16.3 MPa
Strain (perpendicular to texture)	5.16 %	5.17 %	5.08 %
Strain (along texture)	22.8 %	22.0 %	22.8 %

7.3 Video S3: Rotation of MFF in DMSO and MeOH

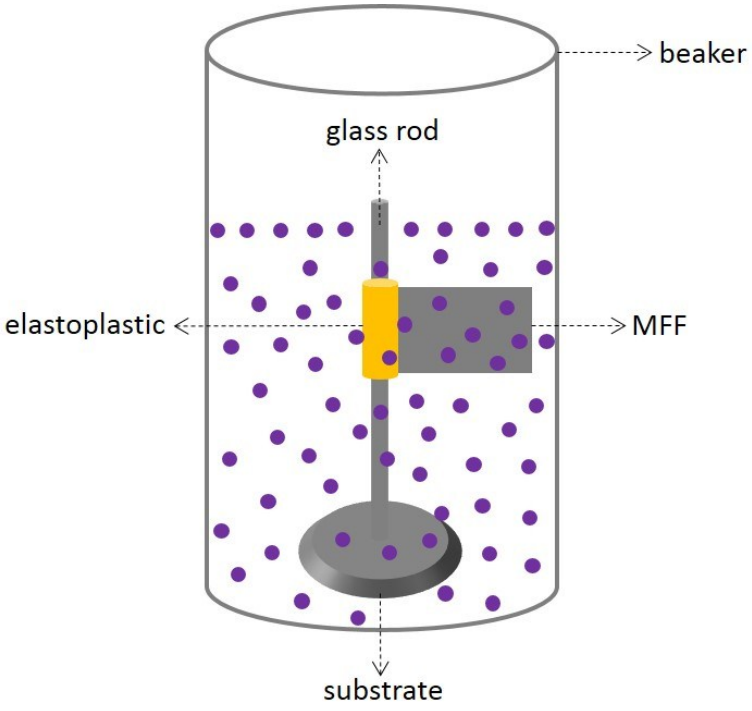

Fig. S14 Experimental set-up for MFF rotation.

As shown in Fig. S14, the glass substrate was equipped with a lathy glass rod, which functioned as a shaft. MFF was clipped onto the elastoplastic tube (orange color) with low weight, which encircled the glass rod. The assembled component was placed into the beaker filled with different solvents (MeOH or DMSO) to induce MFF rotation with the plastic around the glass rod. Video S3 recorded the rotation process of MFF upon solvent adsorption and exchange.

References

1. V. W. Lau, M. B. Mesch, V. Duppel, V. Blum, J. Senker and B. V. Lotsch, *J. Am. Chem. Soc.*, 2015, **137**, 1064.
2. B. Jurgens, E. Irran, J. Senker, P. Kroll, H. Muller and W. Schnick, *J. Am. Chem. Soc.*, 2003, ***34***, 10288.
3. V. A. Davis, A. N. G. Parra-Vasquez, M. J. Green, P. K. Rai, N. Behabtu, V. Prieto, R. D. Booker, J. Schmidt, E. Kesselman, W. Zhow, H. Fan, W. W. Adams, R. H. Hauge, J. E. Fischer, Y. Cohen, Y. Talmon, R. E. Smalley and M. Pasquali, *Nat. Nanotechnol.*, 2009, **4**, 830.
4. N. Behabtu, J. R. Lomeda, M. J. Green, A. L. Higginbotham, A. Sinitskii, D. V. Kosynkin, D. Tsentalovich, A. N. G. Parra-Vasquez, J. Schmidt, E. Kesselman, Y. Cohen, Y. Talmon, J. M. Tour and M. Pasquali, *Nat. Nanotechnol.*, 2010, **5**, 406.
5. Z. Zhou, J. Wang, Y. Shen, Y. Li, A. Liu, S. Liu and Y. Zhang, *J. Am. Chem. Soc.*, 2015, **137**, 2179.
6. A. Sattler, S. Pagano, M. Zeuner, A. Zurawski, D. Gunzelmann, J. Senker, K. Muller-Buschbaum and W. Schnick, *Chem. Eur. J.*, 2009, **15**, 13161.
7. E. Wirnhier, M. B. Mesch, J. Senker and W. Schnick, *Chem. Eur. J.*, 2013, **19**, 2041.
8. C. Pevida, T. C. Drage and C. E. Snape, *Carbon*, 2008, **46**, 1464.
9. M. X. Tan, Y. N. Sum, J. Y. Ying and Y. Zhang, *Energy Environ. Sci.*, 2013, ***6***, 3254.

10. K. Kailasam, Y. S. Jun, P. Katekomol, J. D. Epping, W. H. Hong and A. Thomas, *Chem. Mater.*, 2010, **22**, 428.

11. B. Jurgens, E. Irran, J. Senker, P. Kroll, H. Muller and W. Schnick, *J. Am. Chem. Soc.*, 2003, **125**, 10288.

12. V. W. Lau, M. B. Mesch, V. Duppel, V. Blum, J. Senker and B. V. Lotsch, J. Am. Chem. Soc., 2015, **137**, 1064.

13. C. Huang, J. Wen, Y. Shen, F. Mi, L. He, Z. Gan, J. Ma, S. Liu, H. Ma and Y. Zhang, *Chem. Sci.*, 2018, **9**, 7912.

14. Z. Zhou, J. Wang, Y. Shen, Y. Li, A. Liu, S. Liu and Y. Zhang, *J. Am. Chem. Soc.*, 2015, **137**, 2179.

15. Y. Zhang, A. Thomas, M. Antonietti and X. Wang, *J. Am. Chem. Soc.*, 2009, **131**, 50.

16. R. Fehrmann, N. H. Hansen and N. J. Bjerrum, *Inorg. Chem.*, 1983, **22**, 4009.

17. A. Simon and H. Wagner, *Allg. Chem.*, 1961, **311**, 102.

18. M. Schwanninger, J. C. Rodrigues, H. Pereira and B. Hinterstoisser, *Vib. Spectrosc.*, 2004, **36**, 23.

19. B. Friedel and S. Greulich-Weber, *Small*, 2006, **2**, 859.

20. L. Lin, H. Ou, Y. Zhang and Y. Zhang, *ACS Catal.*, 2016, **6**, 3921.

21. J. G. A. Terlingen, J. Feijen and A. S. Hoffman, *J. Colloid Inter. Sci.*, 1993, **155**, 55.

22. Y. C. Lu, J. Chen, A. J. Wang, N. Bao, J. L. Feng, W. P. Wang and L. Shao, *J. Mater. Chem. C*, 2015, **3**, 73.

23. K. Wang, B. Li, B. Cheng, W. Ho and J. Yu, *Appl. Catal. B-Environ.*, 2015, **176**, 44.

24. G. P. Lopez, D. G. Castner and B. Ratner, *Surf. Interface. Anal.*, 1991, **17**, 267.

25. H. Uehara, S. Diring, S. Furukawa, Z. Kalay, M. Tsotsalas, M. Nakahama, K. Hirai, M. Kondo, O. Sakata and S. Kitagawa, *J. Am. Chem. Soc.*, 2011, **133**, 11932.

26. P. T. Anastas, W. Leitner and P. G. Jessop, *John Wiley & Sons, Inc.*, **2014**, vol. 4, Germany.

27. S. Eshraghi and S. Das, *Acta Biomater.*, **2010**, 6, 2467.